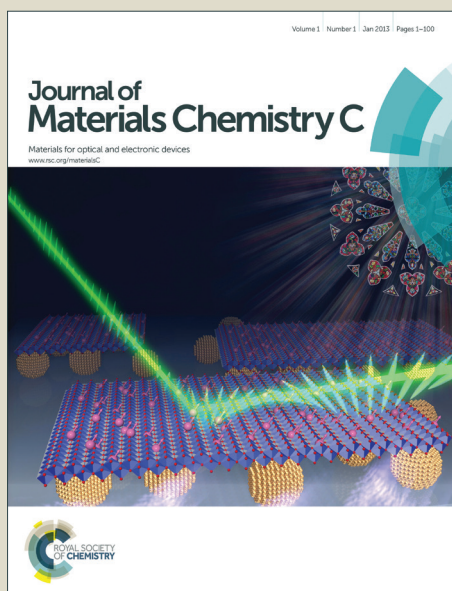


Journal of Materials Chemistry C

Accepted Manuscript



This article can be cited before page numbers have been issued, to do this please use: C. Liu, C. Zheng, X. Liu, Z. CHEN, J. Yang, F. Li, X. Ou and X. Zhang, *J. Mater. Chem. C*, 2014, DOI: 10.1039/C4TC02459A.



This is an *Accepted Manuscript*, which has been through the Royal Society of Chemistry peer review process and has been accepted for publication.

Accepted Manuscripts are published online shortly after acceptance, before technical editing, formatting and proof reading. Using this free service, authors can make their results available to the community, in citable form, before we publish the edited article. We will replace this *Accepted Manuscript* with the edited and formatted *Advance Article* as soon as it is available.

You can find more information about *Accepted Manuscripts* in the [Information for Authors](#).

Please note that technical editing may introduce minor changes to the text and/or graphics, which may alter content. The journal's standard [Terms & Conditions](#) and the [Ethical guidelines](#) still apply. In no event shall the Royal Society of Chemistry be held responsible for any errors or omissions in this *Accepted Manuscript* or any consequences arising from the use of any information it contains.

Multifunctional terpyridine/diphenylamine derivatives as highly efficient blue fluorescent emitters and red phosphorescent hosts

View Article Online
DOI: 10.1039/C4TC02459A

Chuan-Lin Liu,^{a,b} Cai-Jun Zheng,^{*a} Xiao-Ke Liu,^a Zhan Chen,^{a,c} Ji-Ping Yang,^{*b} Fan Li,^a Xue-Mei Ou,^a Xiao-Hong Zhang^{*a,d}

Three terpyridine (TPY)/diphenylamine (DPA) derivatives, with DPA functioning as the electron donor and TPY as the electron acceptor, were designed and synthesized. By switching position of the nitrogen atom in the substituted pyridine of TPY acceptors, we can adjust the electron-drawing strength of TPY group, hence, further modify the fluorescence, lowest unoccupied molecular orbital energy levels, carrier transporting properties of three compounds, but barely influence triplet energy levels. Three compounds satisfy the requirements of multifunctional blue fluorophors and are successfully used as highly efficient blue fluorescent emitters and red phosphorescent hosts in organic light-emitting devices (OLEDs). Non-doped blue fluorescent OLEDs that use TPY22DPA, TPY33DPA, and TPY44DPA as emitters exhibit maximum external quantum efficiencies (EQEs) of 4.9%, 3.8%, and 2.7%, respectively. Meanwhile, red phosphorescent OLEDs that use TPY22DPA, TPY33DPA, and TPY44DPA as host materials exhibit maximum EQEs of 19.1%, 20.9%, and 17.2%, respectively. These results are among the best reported multifunctional blue fluorophor efficiencies.

Introduction

Organic light-emitting devices (OLEDs) have attracted considerable attention because of their potential applications in next-generation full-color flat-panel displays and solid lighting sources.¹ During the past two decades, the exploitation of new OLED emitters² has been greatly successful, particularly for noble metal complex phosphorescent emitters.³ However, given the difficulty of obtaining wide energy gap phosphors, reports regarding highly efficient blue phosphors that can exhibit deep blue emission ($y_{\text{CIE}} < 0.15$, $x_{\text{CIE}} + y_{\text{CIE}} < 0.30$) are insufficient.⁴ In addition, blue phosphorescent devices are typically unstable, which impedes their practical applications. To address these issues, researchers have refocused their attention on blue fluorophors, in which stability and high color purity are readily realized.⁵

Moreover, given the wide energy gaps, blue fluorophors can further realize high triplet energy levels (E_{TS}), hence, have the potential to be used as host materials for red phosphorescent dopants or even orange ones.⁶ Considering this multifunctional property, blue fluorophors can play an important role in reducing the production cost and simplifying the manufacturing process of full-color displays and white lightings.⁷ For instance, Chen et al. synthesized a series of benzimidazole/amine derivatives. By using them as the blue emitters and red phosphorescent hosts, they fabricated blue fluorescent and red phosphorescent OLEDs with maximum EQEs of 1.6% and 7.8%, respectively.^{7a} Based on one of their multifunctional hosts, a simplified white OLED (WOLED) with a maximum EQE of 3% was successfully developed. Meanwhile, Wang et al. reported two metal complexes, namely, $Zn(PPI)_2$ and $Be(PPI)_2$, and demonstrated their multifunction by using them as blue emitters and green/red phosphorescent hosts, respectively.⁸ However, as multifunctional blue fluorophors are still rarely reported, blue fluorescent and red phosphorescent devices both perform poorly based on currently available multifunctional blue fluorophors.^{4a,7,8} The efficiencies of these devices are significantly lower than the 5% and 20% theoretical limits for fluorescent and phosphorescent devices, respectively.^{4a,7-9} Therefore, further development on new highly efficient multifunctional blue fluorophors is highly desirable.

In this work, three terpyridine (TPY)/diphenylamine (DPA) derivatives, namely, 4-[4-(2,2':6',2''-terpyridinyl)]phenyltriphenylamine (TPY22DPA), 4-[4-(3,2':6',3''-terpyridinyl)]phenyltriphenylamine (TPY33DPA), and 4-[4-(4,2':6',4''-terpyridinyl)]phenyltriphenylamine (TPY44DPA), were synthesized as multifunctional blue fluorophors. In these compounds, the well-known hole-transporting moiety DPA was chosen as the electron-donor unit, whereas TPY moieties were used as the electron-acceptor units, considering that Kido et al. proved the outstanding electron-transporting property of the pyridine group.¹⁰ By linking DPA and TPY moieties with a size-appropriate biphenyl- π conjugated bridge, all of the three compounds exhibit efficient blue fluorescence, high E_{TS} , and bipolar transporting properties.¹¹ As shown in Scheme 1, the only difference among the three TPY/DPA derivatives is the various locations of the nitrogen (N) atoms in the substituted pyridine ring. According to our detailed study, the position of the N atom in TPY acceptors can affect the electron-drawing strength of TPY group, thus further modify the fluorescence, lowest unoccupied molecular orbital (LUMO) energy levels, and carrier transporting

properties of three compounds, but barely influence E_{TS} . All three compounds satisfy the requirements of multifunctional blue fluorophors and are successfully used as highly efficient blue fluorescent emitters and red phosphorescent hosts in various devices. Considering performances of both blue and red devices simultaneously, blue fluorescent and red phosphorescent devices based on TPY22DPA can achieve highest efficiencies with maximum EQEs of 4.9% and 19.1%, respectively. These results are among the best reported performance of multifunctional blue fluorophors.

Experimental section

General Procedures. Nuclear magnetic resonance (NMR) spectral data were obtained using a Bruker Advance-400 spectrometer with chemical shifts reported in ppm. Mass spectral data were obtained using a Finnigan 4021C gas chromatography (GC)–mass spectrometry (MS) instrument. Absorption and photoluminescence (PL) spectra were obtained using a Hitachi ultraviolet–visible (UV–Vis) spectrophotometer U-3010 and a Hitachi fluorescence spectrometer F-4600, respectively. Moreover, differential scanning calorimetry (DSC) measurements were acquired using a NETZSCH DSC204 instrument at a heating rate of $10\text{ }^{\circ}\text{C min}^{-1}$ from $20\text{ }^{\circ}\text{C}$ to $420\text{ }^{\circ}\text{C}$ in N_2 atmosphere. Thermogravimetric analysis (TGA) measurements were acquired using a TA Q500 thermogravimeter by measuring the weight loss of the specimens while heating them at a rate of $10\text{ }^{\circ}\text{C min}^{-1}$ from $25\text{ }^{\circ}\text{C}$ to $800\text{ }^{\circ}\text{C}$ in N_2 atmosphere. Lastly, cyclic voltammetry (CV) was performed using a CHI660E electrochemical analyzer.

Synthesis. All commercially available reagents and chemicals were used without further purification. The synthetic routes of TPY22DPA, TPY33DPA, and TPY44DPA are outlined in Scheme 1.

4'-(4-Bromophenyl)-2,2':6,2''-terpyridine (TPY22-Ph-Br). This compound was synthesized according to a modified literature procedure.¹² In a 500 mL round-bottom flask with a magnetic stir bar, NaOH (0.80 g, 20 mmol) and aqueous NH_4OH (100 mL of a 28 wt% solution, 80 mmol) were added into a stirring solution of 4-bromobenzaldehyde (3.70 g, 20 mmol) and 2-acetylpyridine (4.85 g, 40 mmol) in ethanol (150 mL). The resulting mixture was stirred in ambient atmosphere at room temperature for 4 h, during which a precipitate formed. The mixture was then filtered through a Buchner funnel, and the collected precipitate was washed with ethanol (50 mL) and water (100 mL) before being vacuum dried, which yielded a light yellow solid TPY22-Ph-Br (3.21 g) (41%). $^1\text{H NMR}$ (400 MHz, CDCl_3) δ (ppm) 8.85 (d, J =

35.8 Hz, 6H), 8.05 (s, 2H), 7.90 (d, J = 7.9 Hz, 2H), 7.66 (d, J = 8.6 Hz, 2H), 7.52 (s, 2H). MS (EI, m/z): [M]⁺ calcd for C₂₁H₁₄BrN₃, 387.03; found, 387.02.

4-[4-(2, 2': 6', 2''-terpyridinyl)]phenyltriphenylamine (TPY22DPA). In a double-necked 150 mL round-bottom flask with a magnetic stir bar, reflux condenser, and N₂ atmosphere, toluene (12 mL), ethanol (6 mL), and 2 M aqueous Na₂CO₃ (9 mL) were added into a mixture of 4'-(4-bromophenyl)-2,2':6',2''-terpyridine (0.71 g, 2 mmol), 4-(diphenylamino)phenylboronic acid (0.58 g, 2 mmol), and tetrakis(triphenylphosphine)platinum (0.23 g, 0.2 mmol). The mixture was refluxed for 12 h in N₂ inlet. After the mixture cooled to room temperature, the reaction mixture was extracted using dichloromethane and distilled water. The dichloromethane phase was dried over Na₂SO₄ and then filtered. After the solvent was removed under reduced pressure, the crude product was purified through silica gel column chromatography using dichloromethane/methanol (20:1) as eluant. Further purification was achieved via sublimation, which produced a white compound of TPY22DPA (0.84 g) (76%). ¹H NMR (400 MHz, D₆-acetone) δ (ppm) 8.92 (s, 2H), 8.81 – 8.77 (m, 4H), 8.09 – 8.02 (m, 4H), 7.95 (d, J = 8.5 Hz, 2H), 7.76 (d, J = 8.7 Hz, 2H), 7.51 (ddd, J = 7.5, 4.7, 1.3 Hz, 2H), 7.40 – 7.35 (m, 4H), 7.20 – 7.10 (m, 8H). ¹³C NMR (101 MHz, CDCl₃) δ 156.31, 155.95, 149.80, 149.13, 147.65, 147.59, 141.32, 136.90, 136.71, 134.16, 129.35, 127.78, 127.72, 127.05, 124.57, 123.87, 123.75, 123.10, 121.41, 118.67. MS (EI, m/z): [M]⁺ calcd for C₃₈H₂₇N₄, 552.23; found, 552.23.

4'-(4-Bromophenyl)-3,2':6',3''-terpyridine (TPY33-Ph-Br). The same approach for synthesizing TPY22-Ph-Br was followed to obtain the compound of TPY33-Ph-Br (3.62 g) (46%). ¹H NMR (400 MHz, CDCl₃) δ (ppm) 9.40 (d, J = 2.0 Hz, 2H), 8.74 (dd, J = 4.9, 1.5 Hz, 2H), 8.63 (d, J = 8.0 Hz, 2H), 7.96 (s, 2H), 7.71 (d, J = 8.5 Hz, 2H), 7.65 – 7.56 (m, 4H). MS (EI, m/z): [M]⁺ calcd for C₂₁H₁₄BrN₃, 387.03; found, 387.02.

4-[4-(3,2':6',3''-terpyridinyl)]phenyltriphenylamine (TPY33DPA). The same approach for synthesizing and purifying TPY22DPA was followed to obtain the white compound of TPY33DPA (0.92 g) (83%). ¹H NMR (400 MHz, CDCl₃) δ (ppm) 9.45 (s, 2H), 8.77 – 8.70 (m, 4H), 8.07 (s, 2H), 7.83 (d, J = 8.5 Hz, 2H), 7.78 (d, J = 8.4 Hz, 2H), 7.66 (d, J = 5.2 Hz, 2H), 7.56 (d, J = 8.6 Hz, 2H), 7.32 – 7.28 (m, 4H), 7.17 (t, J = 7.2 Hz, 6H), 7.07 (t, J = 7.3 Hz, 2H). ¹³C NMR (101 MHz, CDCl₃) δ 155.41, 150.40, 150.21, 148.45, 147.85, 147.55, 141.89, 136.29, 134.72, 134.56, 133.56, 129.39,

127.76, 127.54, 127.38, 124.70, 123.65, 123.59, 123.26, 117.45. MS (EI, m/z): [M]⁺ calcd for C₃₈H₂₇N₄, 552.23; found, 552.23. View Article Online
DOI: 10.1039/C4TC02459A

4'-(4-Bromophenyl)-4,2':6',4''-terpyridine (TPY44-Ph-Br). The same approach for synthesizing TPY22-Ph-Br was followed to obtain the compound of TPY44-Ph-Br (3.49 g) (46%). ¹H NMR (400 MHz, CDCl₃) δ 8.82 (ppm) (dd, J = 4.6, 1.6 Hz, 4H), 8.15 (d, J = 5.8 Hz, 4H), 8.04 (s, 2H), 7.72 (d, J = 8.5 Hz, 2H), 7.63 (d, J = 8.5 Hz, 2H). MS (EI, m/z): [M]⁺ calcd for C₂₁H₁₄BrN₃, 387.03; found, 387.02.

4-[4-(4,2':6',4''-terpyridinyl)]phenyltriphenylamine (TPY44DPA). The same approach for synthesizing and purifying TPY22DPA was followed to yield the green compound of TPY44DPA (0.91 g) (82%). ¹H NMR (400 MHz, CDCl₃) δ (ppm) 8.83 (s, 4H), 8.20 (d, J = 5.2 Hz, 4H), 8.14 (s, 2H), 7.80 (dd, J = 20.6, 8.4 Hz, 4H), 7.55 (d, J = 8.6 Hz, 2H), 7.32 – 7.27 (m, 4H), 7.17 (t, J = 7.2 Hz, 6H), 7.07 (t, J = 7.3 Hz, 2H). ¹³C NMR (101 MHz, CDCl₃) δ 155.30, 150.68, 150.56, 147.94, 147.52, 146.10, 142.08, 135.98, 133.41, 129.40, 127.76, 127.54, 127.41, 124.73, 123.54, 123.32, 121.22, 118.68. MS (EI, m/z): [M]⁺ calcd for C₃₈H₂₇N₄, 552.23; found, 552.23.

Quantum Calculation. The theoretical calculations of the TPY/DPA derivatives were performed using the Gaussian-09 program. Density functional theory (DFT) B3LPY/6-31G (d) was used to determine and optimize the structures.

Device Fabrication and Measurement. Indium tin oxide (ITO)-coated glasses with a sheet resistance of 30 Ω per square were used as substrates. Before the device was fabricated, the substrates were first cleaned with acetone, ethanol, and deionized water. Then, they were oven-dried at 120 °C and treated with UV-ozone in ambient condition for 5 min. Finally, the cleaned glasses were transferred to a vacuum deposition system at approximately 1 × 10⁻⁶ Torr. Thermally evaporated organic layers were sequentially grown onto the ITO substrates at a rate of 1–2 Å s⁻¹. The cathode was completed via the thermal deposition of lithium fluoride (LiF) at a rate of 0.1 Å s⁻¹ and then covered with aluminum (Al) metal deposited at a rate of 10 Å s⁻¹. Electroluminescence (EL), CIE color coordinates, and spectra were obtained using a Spectrascan PR650 photometer, and the current–voltage characteristics were determined with a computer-controlled Keithley 2400 SourceMeter in ambient atmosphere.

Results and discussion

Synthesis. Scheme 1 illustrates the synthetic routes and molecular structures of TPY22DPA, TPY33DPA, and TPY44DPA. These compounds were synthesized via

the Suzuki cross-coupling reaction between 4-(diphenylamino) phenylboronic acid and 4-bromophenylterpyridine, which were synthesized using acetylpyridine and 4-bromobenzaldehyde. The chemical structures of the three new compounds were fully characterized and confirmed via ^1H , ^{13}C NMR spectroscopy, and MS. Moreover, the TPY/DPA compounds were further purified by sublimation before the device was fabricated.

Thermal Analysis. The thermal properties of the TPY/DPA derivatives were determined through DSC and TGA measurements. As shown in Figure 1 and Table 1, the decomposition temperatures of the three compounds increased in the following order: TPY22DPA (384 °C) < TPY33DPA (403 °C) < TPY44DPA (408 °C), which indicates the increasing polarity and molecular interactions from TPY22DPA to TPY33DPA and TPY44DPA. The glass transition temperature (T_g) of TPY22DPA was observed at 100 °C, which is considerably higher than those of common host materials such as CBP and mCP.¹³ Although no T_g was detected in TPY33DPA and TPY44DPA, both compounds were ensured to have high thermal stabilities because they have similar molecular weights and nearly the same chemical structures with TPY22DPA.

Theoretical Calculations. To gain insight into the structure–property relationship of the TPY/DPA derivatives at the molecular level, DFT calculations were performed in TPY22DPA, TPY33DPA, and TPY44DPA, as shown in Figure 2. The calculations suggest that the three TPY/DPA compounds have similar distributions at the highest occupied molecular orbital (HOMO) and LUMO. HOMOs are primarily located at the DPA unit and the biphenyl π bridge because of the strong electron-donating character of the DPA unit. In LUMOs, however, electron distributions are mostly located at the electron-deficient TPY moieties and the biphenyl π bridge. The separation between these two orbitals maintains the individual electronic properties of the functional groups and benefits efficient hole- and electron-transporting molecular properties. Moreover, a suitable LUMO–HOMO overlap can provide an efficient intramolecular charge transfer (ICT) transition emission and high E_{TS} to the three compounds.¹⁴

Electrochemical Properties. The electrochemical properties of the TPY/DPA derivatives were investigated via CV in dimethylformamide. HOMO/LUMO energy levels were calculated based on ferrocene (with a Fermi level of 5.10 eV according to literature¹⁵). As shown in Figure 3, the three TPY/DPA compounds presented irreversible oxidation curves, which possibly originated from the electron-rich DPA

unit. Based on the estimated onset potentials of the oxidation curves, the HOMO energy levels of TPY22DPA, TPY33DPA, and TPY44DPA were -5.54 , -5.52 , and -5.50 eV, respectively. Similar HOMO levels can also confirm the occurrence of oxidation in the DPA units of the three compounds. During the reduction process, quasi-reversible curves were observed in the three compounds, which can be attributed to the electron-deficient TPY moieties. The LUMO energy levels of TPY22DPA, TPY33DPA, and TPY44DPA were reduced to -2.83 , -2.86 , and -2.93 eV from the onset potentials of the reduction curves. From TPY22DPA to TPY33DPA and TPY44DPA, the lower and lower LUMO energy levels indicate that the positions of the N atoms in the substituted pyridine rings can affect the electron-deficient level of TPY moiety. The 4, 4''-positioned TPY moiety can draw electrons most effectively.

Photophysical Properties. The UV-vis absorption and PL spectra of the three TPY/DPA derivatives in the diluted ethyl acetate solution are shown in Figure 4a. The three compounds exhibited similar absorption behaviors in the ethyl acetate solution. The absorption peaks at 270 nm are associated with the DPA-centered $n-\pi^*$ transition,¹⁶ whereas the long wavelength peaks at approximately 360 nm are attributed to ICT transition from the electron-rich DPA moiety to the electron-deficient TPY core. Unlike their absorption behaviors, the three TPY/DPA derivatives displayed slightly red-shifted blue emissions with peaks at 460, 470, and 487 nm for TPY22DPA, TPY33DPA, and TPY44DPA in ethyl acetate solution, respectively. The red-shifted fluorescence from TPY22DPA to TPY33DPA and TPY44DPA can be attributed to the different electron-deficient levels of TPY moieties in molecules, which can be verified through the HOMO/LUMO energy levels of the three compounds. As shown in Figure 4b, the shift trend was maintained in the PL spectra of the three compounds in thin solid films, wherein the spectrum peaks were at 455, 465, and 475 nm for TPY22DPA, TPY33DPA, and TPY44DPA, respectively. The respective fluorescent quantum yields (Φ_f) of TPY22DPA, TPY33DPA, and TPY44DPA were 0.76, 0.67, and 0.59 in the ethyl acetate solution, which were measured using quinine bisulfate ($\Phi_f = 0.546$ in 1 M H_2SO_4)¹⁷ as the standard. In neat thin solid film, these values still remain at high levels of 0.45, 0.42, and 0.42 for TPY22DPA, TPY33DPA, and TPY44DPA respectively. The high values of Φ_f indicate that our TPY/DPA derivatives are excellent blue fluorescent emitters. The phosphorescent spectra of the three TPY/DPA derivatives were investigated in 2-

methyltetrahydrofuran glass at 77 K. As shown in Figure 4c, the nearly similar phosphorescent spectra of the derivatives indicate that the T_1 states of the three compounds are located mostly in the electron-donating DPA moiety.¹⁸ Based on the peaks of the phosphorescent spectra, E_{T_1} s were estimated as 2.44, 2.43, and 2.43 eV for TPY22DPA, TPY33DPA, and TPY44DPA, respectively. The similar triplet energy results indicate that the positions of the N atoms in the substituted pyridine rings do not influence the T_1 states of the three compounds. The high E_{T_1} s are sufficient for sensitizing phosphorescent dopants with E_{T_1} s that are below 2.40 eV.¹⁹ Therefore, our novel TPY/DPA derivatives are applicable as blue emitters and red phosphorescent hosts.

Electroluminescence Performance. Non-doped blue fluorescent OLEDs were initially fabricated using a device structure of ITO/TAPC (50 nm)/TCTA (5 nm)/TPY/DPA (30 nm)/TmPyPB (45 nm)/LiF (1 nm)/Al (120 nm). Devices B1, B2, and B3 represent OLEDs that use TPY22DPA, TPY33DPA, and TPY44DPA as the emitting layer (EML), respectively. In these devices, ITO and LiF/Al are the anode and cathode, respectively. TAPC (4,4'-cyclohexylidenebis[N,N2bis(4-methylphenyl)benzenamine]) is the hole-transporting layer. TCTA (4,4',4''-tris(N-carbazolyl)triphenylamine) is the exciton-blocking layer. TmPyPB (1,3,5-tri[(3-pyridyl)-phen-3-yl]benzene) is the electron-transporting, hole-blocking, and exciton-blocking layers. The non-doped blue devices based on TPY22DPA, TPY33DPA, and TPY44DPA exhibit stable blue fluorescent spectra with different luminances; peaks at 448, 460, and 476 nm; and CIE coordinates of (0.15, 0.11), (0.15, 0.17), and (0.17, 0.26), respectively. As shown in Figure S1, devices B1, B2, and B3 exhibit significantly low turn-on voltages of 3, 2.6, and 2.7 V, respectively, which nearly reach the energy limit of blue OLEDs. An important reason for such low turn-on voltages is the suitable HOMO and LUMO energy levels of the three compounds. As shown in Figure 7, only small carrier injection barriers exist in the holes and electrons because of the bipolar transporting property of blue fluorophors. To further prove this property, we fabricated hole-only and electron-only devices using the ITO/MoO₃ (12 nm)/TPY/DPA (60 nm)/MoO₃ (12 nm)/Al and ITO/Al (60 nm)/TPY/DPA (60 nm)/Al structures, respectively. As shown in Figure 6, all non-doped carrier-only devices based on the three compounds exhibited remarkable current densities, which proved the bipolar transporting property of the three TPY/DPA derivatives. Moreover, with the increasing electron-deficient level of

TPY moieties, the electron mobilities of the three compounds increased rapidly from TPY22DPA to TPY33DPA and TPY44DPA, whereas hole mobilities exhibited the opposite result. Accordingly, TPY22DPA displayed the best ambipolar transporting property with nearly similar current densities for holes and electrons. Therefore, as shown in Figure 5a, device B1 exhibited the highest efficiency and lowest efficiency roll-off. As shown in Table 2, device B1 exhibited maximum efficiencies of 4.4 lm W⁻¹ for power efficiency (PE), 5.6 cd A⁻¹ for current efficiency (CE), and 4.9% for EQE. Such high efficiencies are also attributed to the highest Φ_f of TPY22DPA in neat thin films. Considering the 5% theoretical limit for fluorescent devices, TPY22DPA is deemed as an outstanding blue fluorophor.^{9b}

To verify the host properties of the three compounds for red phosphors, phosphorescent devices were constructed based on the TPY/DPA derivatives. The devices have similar configurations of ITO /TAPC (50 nm)/TCTA (5 nm)/TPY/DPA: 2% Ir(MDQ)₂acac (30 nm)/TmPyPB (45 nm)/LiF (1 nm)/Al (120 nm). Devices R1, R2, and R3 were used with TPY22DPA, TPY33DPA, and TPY44DPA, respectively. The Ir(MDQ)₂acac used in this study was iridium(III)bis(2-methyldibenzo[f,h]quinoxaline)(acetylacetonate). As shown in Figure S2, devices R1, R2, and R3 have low turn-on voltages of 2.9, 2.4, and 2.5 V, respectively. These turn-on voltages, which are lower than those for non-doped blue devices, can be attributed to the trapping effect of the red dopant Ir(MDQ)₂acac. As shown in Table 2, the maximum EQE, PE and CE were 19.1%, 40.2 lm W⁻¹ and 38.5 cd A⁻¹, respectively, for device R1; 20.9 %, 53.6 lm W⁻¹ and 42.7 cd A⁻¹, respectively, for device R2; as well as 17.2 %, 37.2 lm W⁻¹ and 35.5 cd A⁻¹, respectively, for device R3. The outstanding results can be ascribed to the perfect energy transfer from the hosts to the dopants, which has been demonstrated by the high Φ_f s of the host films doped with a phosphorescent emitter, *i.e.* 0.89 for 2% Ir(MDQ)₂acac doped in TPY22DPA, 0.86 for 2% Ir(MDQ)₂acac doped TPY33DPA, and 0.85 for 2% Ir(MDQ)₂acac doped TPY44DPA, respectively. Considering the 20% theoretical limit for EQE in phosphorescent devices,^{9a} the three devices exhibited extremely high EQEs, which indicate that the TPY/DPA derivatives are not only efficient blue fluorescent emitters, but also perform remarkably for red phosphors. According to Figure 5c, device R2 exhibited the highest efficiency and lowest efficiency roll-off, which is in contrast to those of non-doped blue fluorescent devices. To understand this result, doped carrier-only devices were constructed based on the three hosts. Through the trapping effect of

the red dopant Ir(MDQ)₂acac, the carrier transporting properties of doped EMLs significantly differed from those of non-doped EMLs. As shown in Figure 6, the Ir(MDQ)₂acac of doped TPY33DPA exhibited an ambipolar transporting property, and thus, achieved the best performance. Considering all the results of non-doped blue fluorescent and red phosphorescent devices, TPY22DPA performed the best among the three derivatives and achieved the best results for reported multifunctional blue fluorophors (Table S1).

To further prove the superiority of our multifunctional blue fluorophors, a WOLED (device W) was fabricated based on TPY22DPA using the configuration of ITO/TAPC (50 nm)/TCTA (5 nm)/TPY22DPA:0.1% Ir(MDQ)₂acac (30 nm)/TmPyPB (45 nm)/LiF (1 nm)/Al (120 nm). In this device, based on appropriate doping concentration, the singlet and triplet excitations generated in EML can be successfully separated and respectively utilized by TPY22DPA and red phosphorescent dopants. As a result, TPY22DPA had dual roles as both an efficient blue emitter and an excellent red phosphor host. The device exhibited a warm white emission with a CIE value of (0.43, 0.34) at 1000 cd m⁻². Moreover, the max forward-viewing EQE of 19.3% and the PE of 38.6 lm W⁻¹ were achieved in this device (Figure 8). The single-doped device structure is considerably simpler than the stacked, multi-emissive layer or multi-doped WOLEDs. This white device proved that our multifunctional blue fluorophor TPY22DPA can reduce production cost and simplify the manufacturing process for such devices, particularly for WOLEDs.

Conclusion

In summary, a series of multifunctional TPY/DPA derivatives, namely, TPY22DPA, TPY33DPA, and TPY44DPA, were designed and synthesized. By switching position of the N atom in the substituted pyridine of TPY acceptors, we can adjust the electron-drawing strength of TPY group, thus, further modify the fluorescence, LUMO energy levels, and carrier transporting properties of three compounds, but barely affect triplet energy levels. The non-doped blue devices based on TPY22DPA, TPY33DPA, and TPY44DPA exhibited high maximum EQEs of 4.9%, 3.8%, and 2.7%, respectively, whereas the red phosphorescent device hosts based on TPY22DPA, TPY33DPA, and TPY44DPA exhibited high maximum EQEs of 19.1%, 20.9%, and 17.2%, respectively. These results illustrate that the TPY/DPA derivatives are the most excellent blue fluorescent emitters and are outstanding host materials for red phosphorescent dopants. Furthermore, our work also successfully presents a

simple design strategy for further and precisely adjusting the properties of multifunctional blue fluorophors.

View Article Online

DOI: 10.1039/C4TC02459A

Acknowledgements

This work was supported by the National Natural Science Foundation of China (Grant No. 51373190, 51033007, 51103169, 21174009), the Beijing Nova Program (Grant No. Z14110001814067) and the Instrument Developing Project of the Chinese Academy of Sciences (Grant No. YE201133), P. R. China.

Notes and reference

^a*Nano-organic Photoelectronic Laboratory and Key Laboratory of Photochemical Conversion and Optoelectronic Materials, Technical Institute of Physics and Chemistry, Chinese Academy of Sciences, Beijing 100190, P.R. China. Fax: +86-10-64879375; Tel: +86-10-82543510; E-mail: xhzhang@mail.ipc.ac.cn, zhengcaijun@mail.ipc.ac.cn*

^b*Key Laboratory of Aerospace Advanced Materials and Performance, Ministry of Education, School of Materials Science and Engineering, Beihang University, Beijing 100191, P.R. China. E-mail: jyang@buaa.edu.cn*

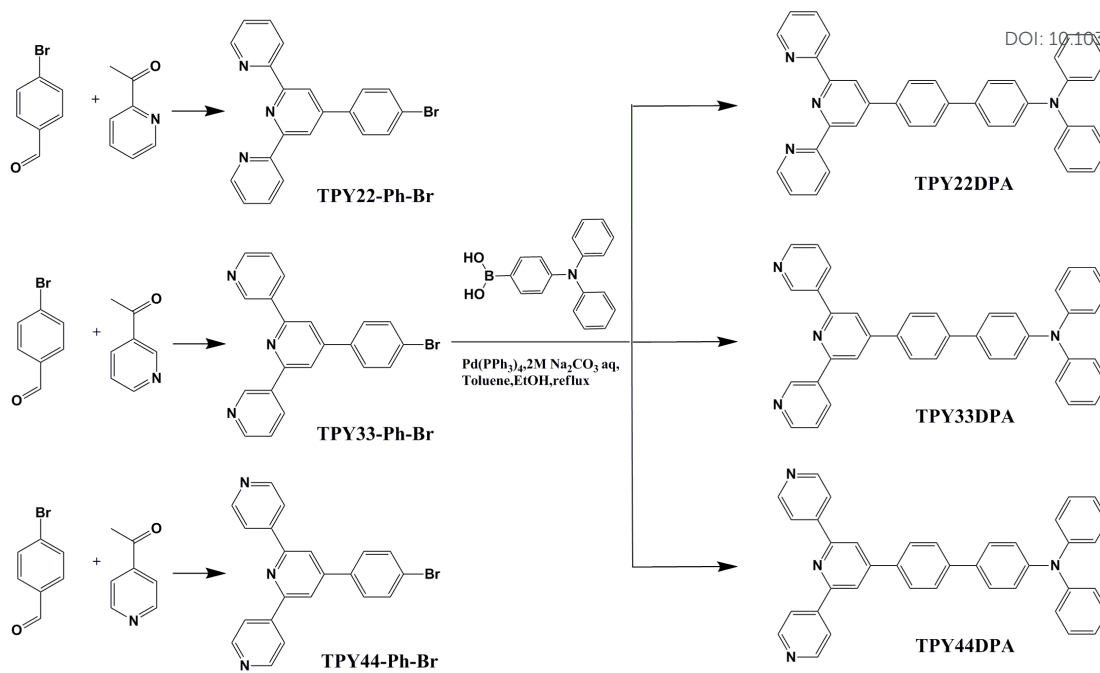
^c*University of Chinese Academy of Sciences, Beijing 100039, P.R. China.*

^d*Functional Nano & Soft Materials Laboratory (FUNSOM) Jiangsu Key Laboratory for Carbon-Based Functional Materials & Devices and Collaborative Innovation Center of Suzhou Nano Science and Technology, Soochow University Suzhou, Jiangsu 215123 (P. R. China)*

(1) (a) B.-H. Zhang, G.-P. Tan, C.-S. Lam, B. Yao, C.-L. Ho, L.-H. Liu, Z.-Y. Xie, W.-Y. Wong, J.-Q. Ding, L.-X. Wang, *Adv Mater.* 2012, **24**, 1873; (b) R.-J. Wang, D. Liu, H.-C. Ren, T. Zhang, H.-M. Yin, G.-Y. Liu, J.-Y. Li, *Adv Mater.* 2011, **23**, 2823; (c) S. Reineke, F. Lindner, G. Schwartz, N. Seidler, K. Walzer, B. Lussem, K. Leo, *Nature.* 2009, **459**, 234.

- (2) (a) X.-K. Liu, C.-J. Zheng, M.-F. Lo, J. Xiao, Z. Chen, C.-L. Liu, C.-S. Lee, M.-K. Fung, X.-H. Zhang, *Chem Mater.* 2013, **25**, 4454; (b) Y.-C. Zhu, L. Zhou, H.-Y. Li, Q.-L. Xu, M.-Y. Teng, Y.-X. Zheng, J.-L. Zuo, H.-J. Zhang, X.-Z. You, *Adv Mater.* 2011, **23**, 4041; (c) Y. Yuan, J.-X. Chen, F. Lu, Q.-X. Tong, Q.-D. Yang, H.-W. Mo, T.-W. Ng, F.-L. Wong, Z.-Q. Guo, J. Ye, Z. Chen, X.-H. Zhang, C.-S. Lee, *Chem Mater.* 2013, **25**, 4957.
- (3) (a) A. Kohler, J.-S. Wilson, R.-H. Friend, *Adv Mater.* 2002, **14**, 701; (b) C.-H. Fan, P.-P. Sun, T.-H. Su, C.-H. Cheng, *Adv Mater.* 2011, **23**, 2981.
- (4) (a) M.-Y. Lai, C.-H. Chen, W.-S. Huang, J.-T. Lin, T.-H. Ke, L.-Y. Chen, M.-H. Tsai, C.-C. Wu, *Angew Chem Int Edit.* 2008, **47**, 581. (b) R.-J. Holmes, S.-R. Forrest, T. Sajoto, A. Tamayo, P.-I. Djurovich, M.-E. Thompson, J. Brooks, Y.-J. Tung, B.-W. D'andrade, M.-S. Weaver, R.-C. Kwong, J.-J. Brown, *Appl Phys Lett.* 2005, **87**; (c) C.-H. Yang, Y.-M. Cheng, Y. Chi, C.-J. Hsu, F.-C. Fang, K.-T. Wong, P.-T. Chou, C.-H. Chang, M.-H. Tsai, C.-C. Wu, *Angew Chem Int Edit.* 2007, **46**, 2418.
- (5) (a) M.-R. Zhu, C.-L. Yang, *Chem Soc Rev.* 2013, **42**, 4963; (b) R. Kim, S. Lee, K.-H. Kim, Y.-J. Lee, S.-K. Kwon, J.-J. Kim, Y.-H. Kim, *Chem Commun.* 2013, **49**, 4664; (c) J. Ye, Z. Chen, M.-K. Fung, C.-J. Zheng, X.-M. Ou, X.-H. Zhang, Y. Yuan, C.-S. Lee, *Chem Mater.* 2013, **25**, 2630; (d) Y. Zou, J.-H. Zou, T.-L. Ye, H. Li, C.-L. Yang, H.-B. Wu, D.-G. Ma, J.-G. Qin, Y. Cao, *Adv Funct Mater.* 2013, **23**, 1781; (e) C. Liu, Y.-H. Li, Y.-F. Li, C.-L. Yang, H.-B. Wu, J.-G. Qin, Y. Cao, *Chem Mater.* 2013, **25**, 3320.
- (6) (a) T. Zhang, D. Liu, Q. Wang, R.-J. Wang, H.-C. Ren, J.-Y. Li, *J Mater Chem.* 2011, **21**, 12969; (b) S.-L. Gong, Y.-B.-A. Zhao, M. Wang, C.-L. Yang, C. Zhong, J.-G. Qin, D.-G. Ma, *Chemistry-an Asian Journal.* 2010, **5**, 2093.
- (7) (a) C.-H. Chen, W.-S. Huang, M.-Y. Lai, W.-C. Tsao, J.-T. Lin, Y.-H. Wu, T.-H. Ke, L.-Y. Chen, C.-C. Wu, *Adv Funct Mater.* 2009, **19**, 2661; (b) Y.-T. Tao, Q. Wang, Y. Shang, C.-L. Yang, L. Ao, J.-G. Qin, D.-G. Ma, Z.-G. Shuai, *Chem Commun.* 2009, 77.
- (8) K. Wang, F.-C. Zhao, C.-G. Wang, S.-Y. Chen, D. Chen, H.-Y. Zhang, Y. Liu, D.-G. Ma, Y. Wang, *Adv Funct Mater.* 2013, **23**, 2672.
- (9) (a) C. Adachi, M.-A. Baldo, M.-E. Thompson, S.-R. Forrest, *J Appl Phys.* 2001, **90**, 5048. (b) C.-G. Zhen, Y.-F. Dai, W.-J. Zeng, Z. Ma, Z.-K. Chen, J. Kieffer, *Adv Funct Mater.* 2011, **21**, 699.

- (10) (a) S.-J. Su, T. Chiba, T. Takeda, J Kido. *Adv Mater.* 2008, **20**, 2125. (b) H. Sasabe, D. Tanaka, D. Yokoyama, T. Chiba, Y.-J. Pu, K. Nakayama, M. Yokoyama, J. Kido, *Adv Funct Mater.* 2011, **21**, 336. View Article Online
DOI: 10.1039/C4TC02459A
- (11) (a) J. Ye, C.-J. Zheng, X.-M. Ou, X.-H. Zhang, M.-K. Fung, C.-S. Lee, *Adv Mater.* 2012, **24**, 3410. (b) C.-J. Zheng, J. Wang, J. Ye, M.-F. Lo, X.-K. Liu, M.-K. Fung, X.-H. Zhang, C.-S Lee, *Adv Mater.* 2013, **25**, 2205. (c) X.-K. Liu, C.-J. Zheng, M.-F. Lo, J. Xiao, C.-S. Lee, M.-K. Fung, X.-H. Zhang, *Chem Commun.* 2014, **50**, 2027.
- (12) J.-H. Wang, G.-S. Hanan, *Synlett.* 2005, 1251.
- (13) (a) M.-H. Tsai, Y.-H. Hong, C.-H. Chang, H.-C. Su, C.-C. Wu, A. Matoliukstyte, J. Simokaitiene, S. Grigalevicius, J.-V. Grazulevicius, C.-P. Hsu, *Adv Mater.* 2007, **19**, 862; (b) F.-M. Hsu, C.-H. Chien, Y.-J. Hsieh, C.-H. Wu, C.-F. Shu, S.-W. Liu, C.-T. Chen, *J Mater Chem.* 2009, **19**, 8002.
- (14) W.-J. Li, D.-D. Liu, F.-Z. Shen, D.-G. Ma, Z.-M. Wang, T. Feng, Y.-X. Xu, B. Yang, Y.-G. Ma, *Adv Funct Mater.* 2012, **22**, 2797.
- (15) C.-M. Cardona, W. Li, A.-E. Kaifer, D. Stockdale, G.-C. Bazan, *Adv Mater.* 2011, **23**, 2367.
- (16) Y.-T. Tao, Q. Wang, C.-L. Yang, C. Zhong, K. Zhang, J.-G. Qin, D.-G. Ma, *Adv Funct Mater.* 2010, **20**, 304.
- (17) D.-F. Eaton, *Pure Appl Chem.* 1988, **60**, 1107.
- (18) Q.-S. Zhang, J. Li, K. Shizu, S.-P. Huang, S. Hirata, H. Miyazaki, C. Adachi, *J Am Chem Soc.* 2012, **134**, 14706.
- (19) J.-P. Duan, P.-P. Sun, C.-H. Cheng, *Adv Mater.* 2003, **15**, 224.



Scheme 1. Synthetic Routes and Chemical Structures of TPY22DPA, TPY33DPA, and TPY44DPA.

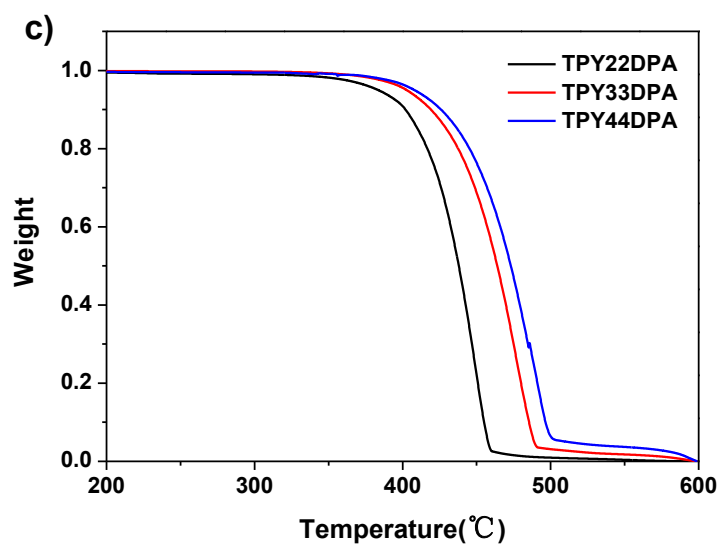
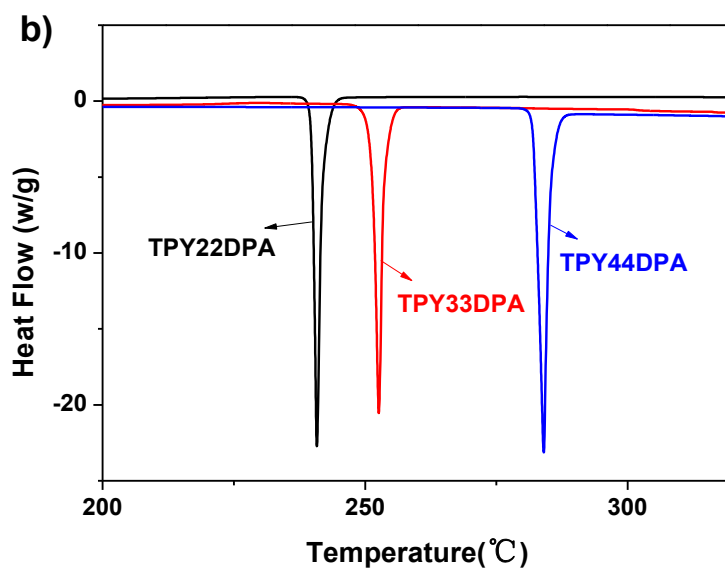
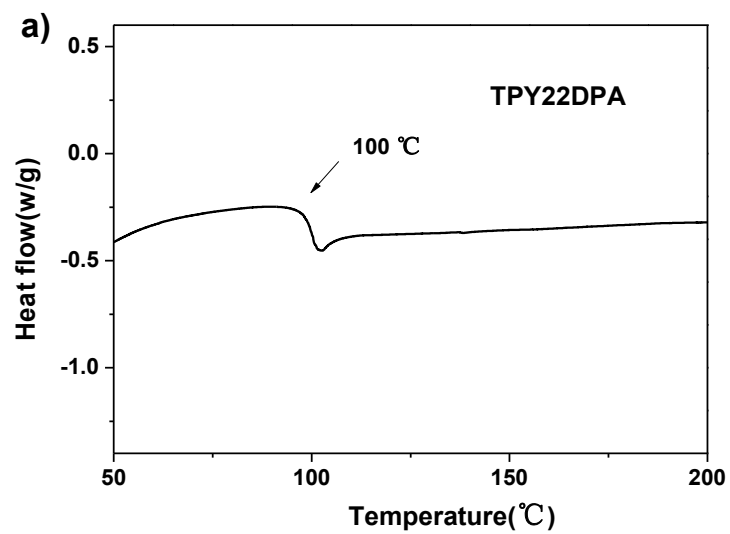
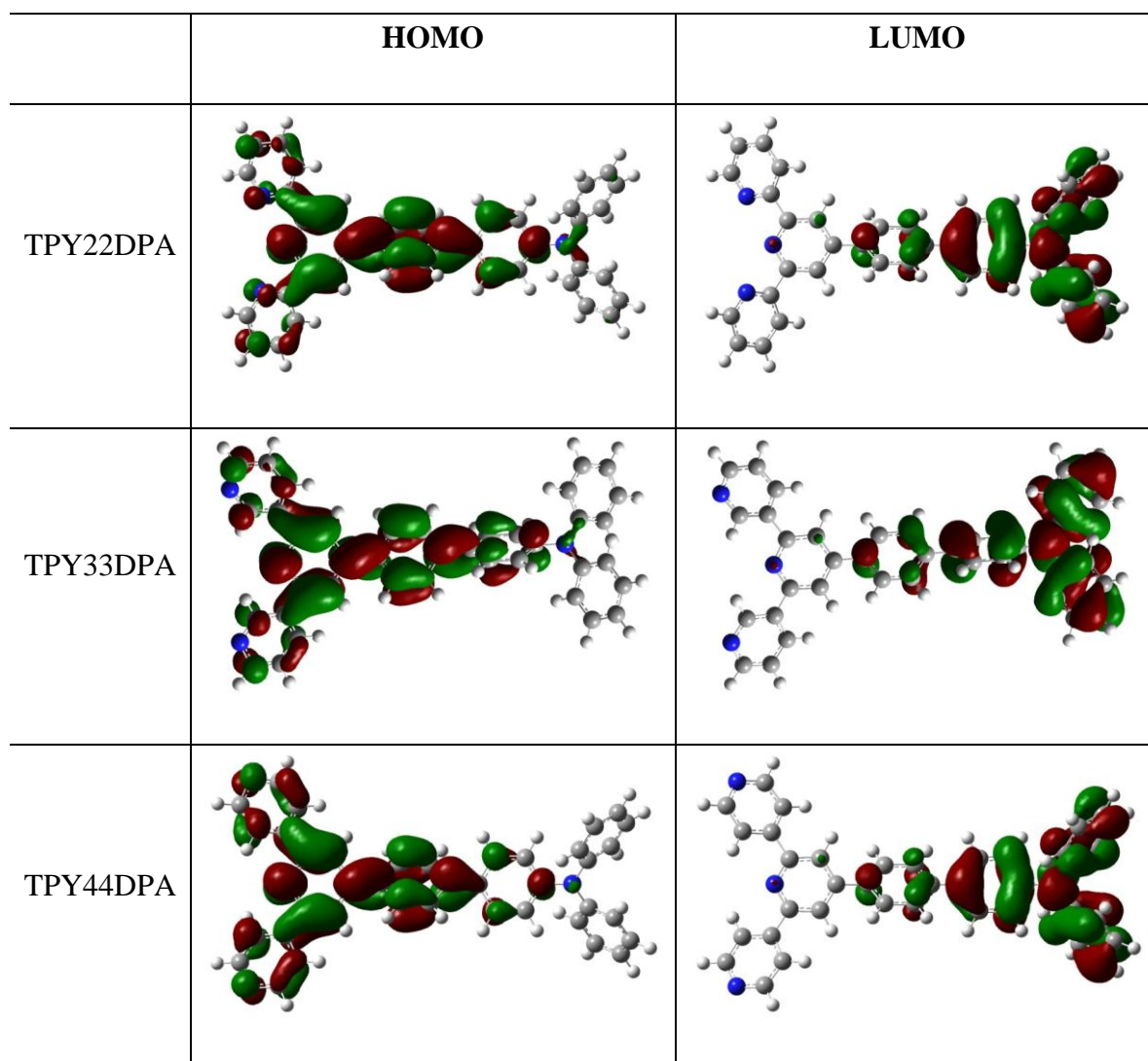


Figure 1. DSC and TGA thermograms of TPY22DPA, TPY33DPA, and TPY44DPA. View Article Online
DOI: 10.1039/C4TC02459A**Figure 2.** Calculated spatial distributions of the HOMO/LUMO of TPY22DPA, TPY33DPA, and TPY44DPA.

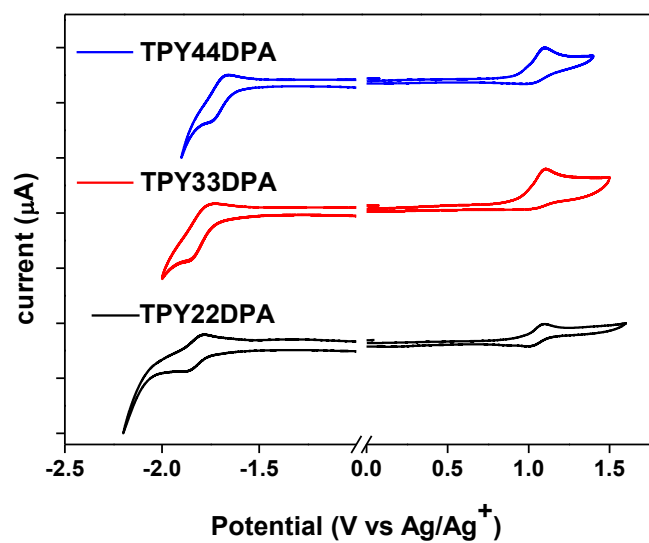


Figure 3. Cyclic voltammograms of TPY22DPA, TPY33DPA, and TPY44DPA in DMF.

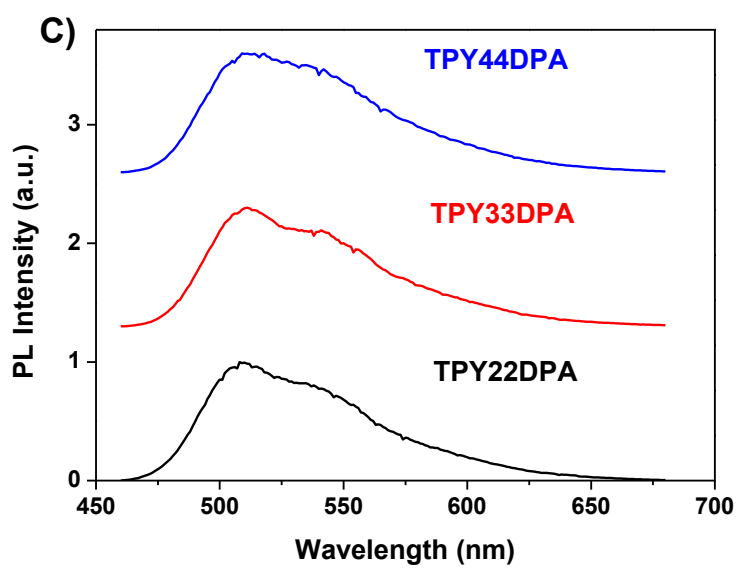
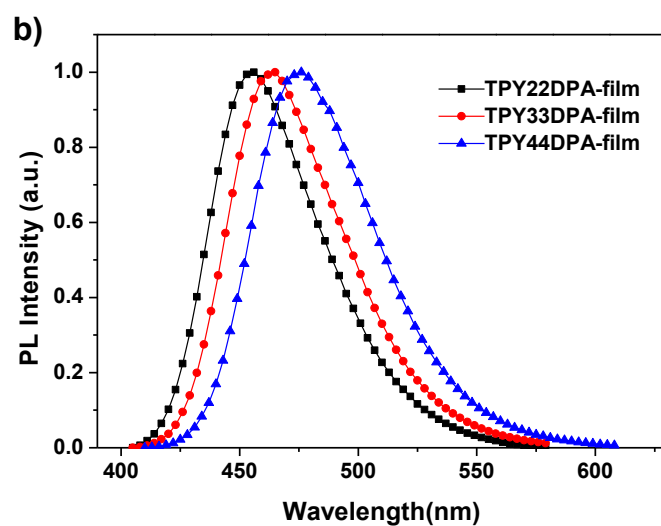
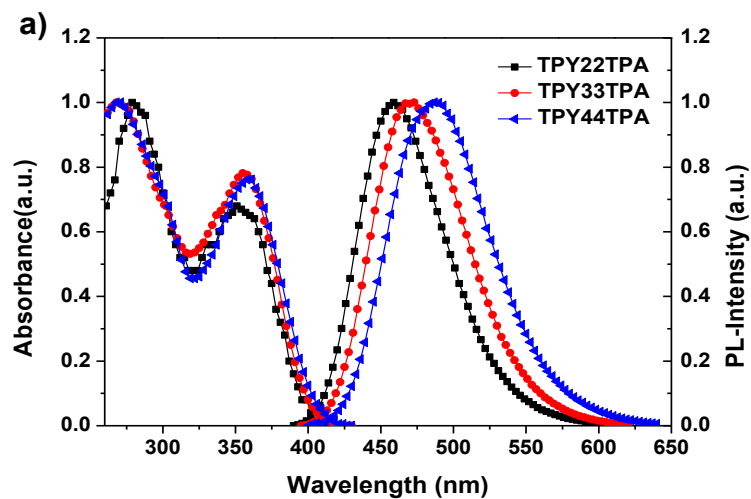


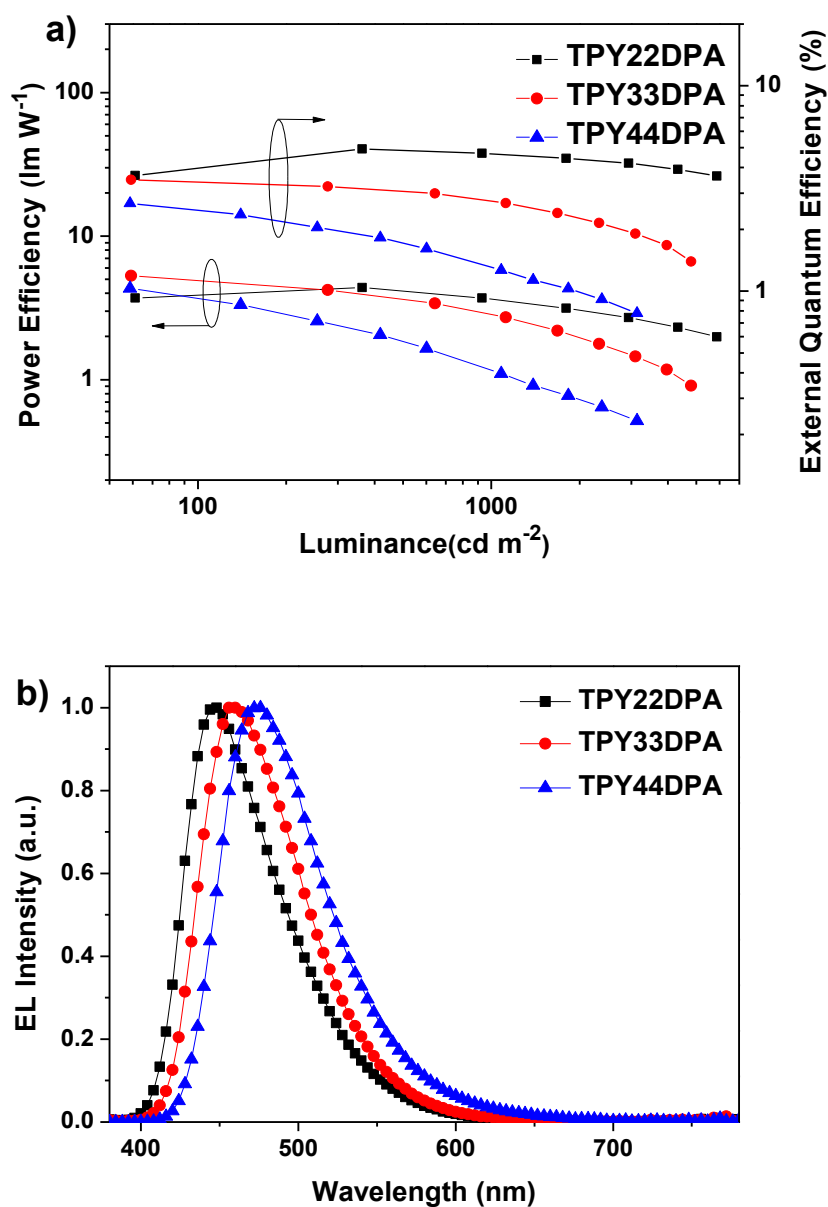
Figure 4. a) UV-vis absorption and PL spectra of TPY22DPA, TPY33DPA, and TPY44DPA in ethyl acetate solution at room temperature. (b) PL spectra of TPY22DPA, TPY33DPA, and TPY44DPA in solid film at room temperature. c) The phosphorescence spectra of TPY22DPA, TPY33DPA, and TPY44DPA in 2-methyltetrahydrofuran at 77K.

New Article Online
DOI: 10.1039/C4TC02459A

Table 1 Summary of the Physical Properties of TPY22DPA, TPY33DPA, and TPY44DPA

Materials	$\lambda_{\text{abs}}^{\text{a}}$ (nm)	$\lambda_{\text{PL}}^{\text{a}}$ (nm)	$\lambda_{\text{PL}}^{\text{b}}$ (nm)	$\Phi_{\text{f}}^{\text{a}}$	E_{T}^{c} (eV)	LUMO ^d (eV)	HOMO ^d (eV)	T_{g} ($^{\circ}\text{C}$)	T_{m} ($^{\circ}\text{C}$)	T_{d} ($^{\circ}\text{C}$)
TPY22DPA	281,350	460	455	0.76	2.44	-2.83	-5.54	100	241	384
TPY33DPA	272,356	470	465	0.67	2.43	-2.86	-5.52	- ^e	253	403
TPY44DPA	270,360	487	475	0.59	2.42	-2.93	-5.5	- ^e	284	408

^aMeasured in Ethyl acetate solution (10^{-5}M); ^bMeasured in thin solid film; ^cTriplet energy measured in 2-MeTHF at 77K (10^{-5}M); ^dLUMO and HOMO was measured from the onset of reduction and oxidation potentials; ^eNot observed.



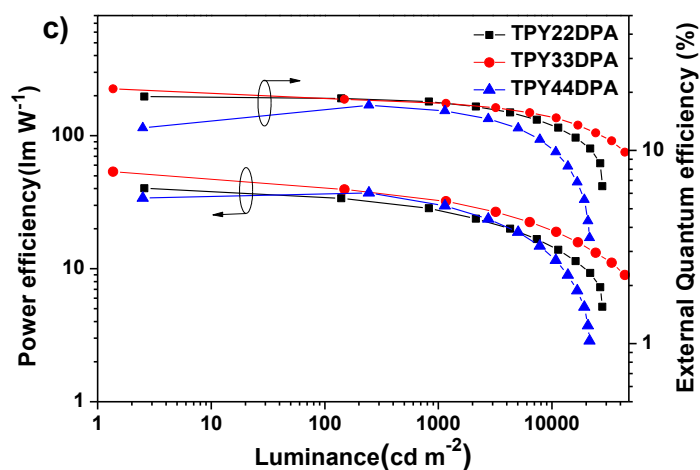


Figure 5. a) PE-EQE-Luminance plots of device B1, B2, and B3. b) The EL spectra of device B1, B2, and B3. c) PE-EQE-Luminance plots of device R1, R2, and R3.

Table 2. The Electroluminescent Properties of the Devices

Device	V_{on} (V)	Max			1000 $cd\ m^{-2}$			CIE
		CE ($cd\ A^{-1}$)	PE ($lm\ W^{-1}$)	EQE (%)	CE ($cd\ A^{-1}$)	PE ($lm\ W^{-1}$)	EQE (%)	
B1	3.0	5.6	4.4	4.9	5.3	3.7	4.7	(0.15,0.11)
B2	2.6	5.3	5.6	3.8	4.5	3.5	3.2	(0.15,0.17)
B3	2.7	5.0	5.2	2.8	2.3	1.1	1.3	(0.16,0.26)
R1	2.9	38.5	40.2	19.1	36.2	28.4	17.9	(0.60,0.40)
R2	2.4	42.7	53.6	20.9	35.9	32.2	17.6	(0.59,0.40)
R3	2.5	35.5	37.2	17.2	30.5	23.9	15.0	(0.59,0.40)

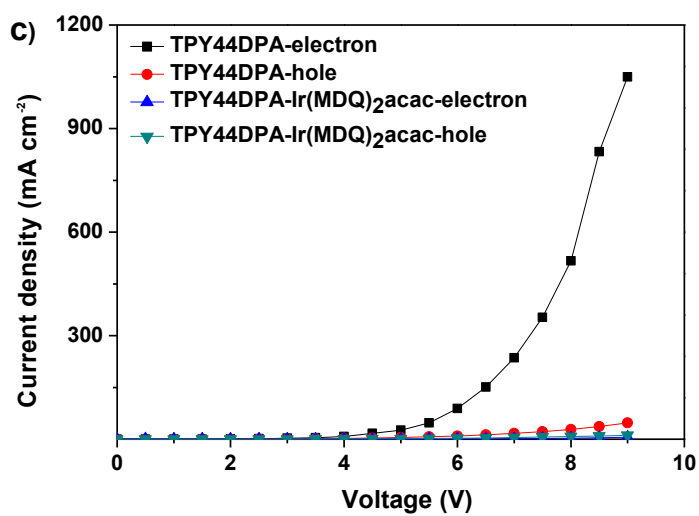
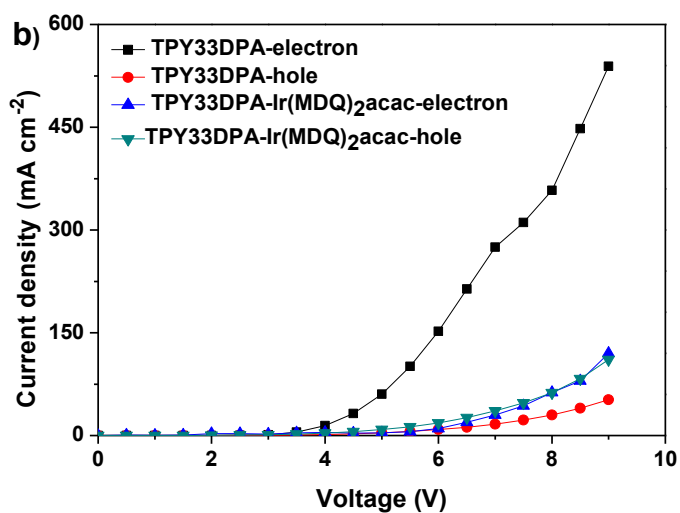
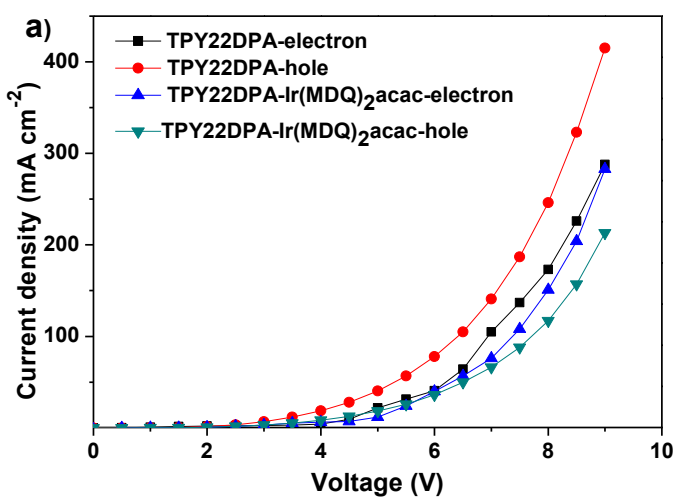


Figure 6. Current density versus voltage characteristics of the hole-only and electron-only devices for a) TPY22DPA and TPY22DPA with 2%Ir(MDQ)₂acac; b) TPY33DPA and TPY33DPA with 2%Ir(MDQ)₂acac; c) TPY44DPA and TPY44DPA with 2%Ir(MDQ)₂acac.

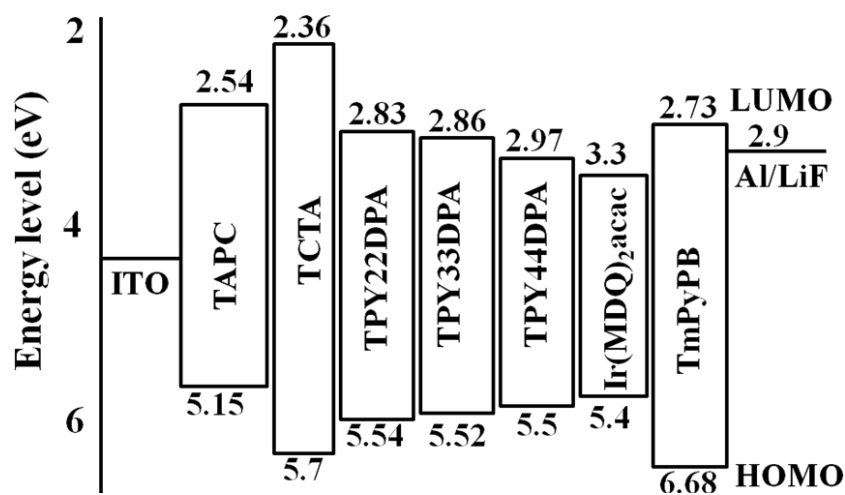
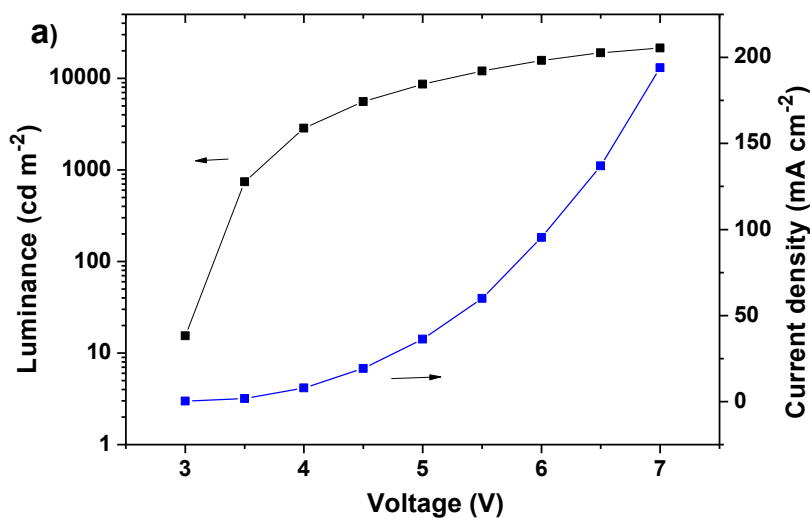


Figure 7. Energy level diagram of the devices based on the TPY22DPA, TPY33DPA, and TPY44DPA.



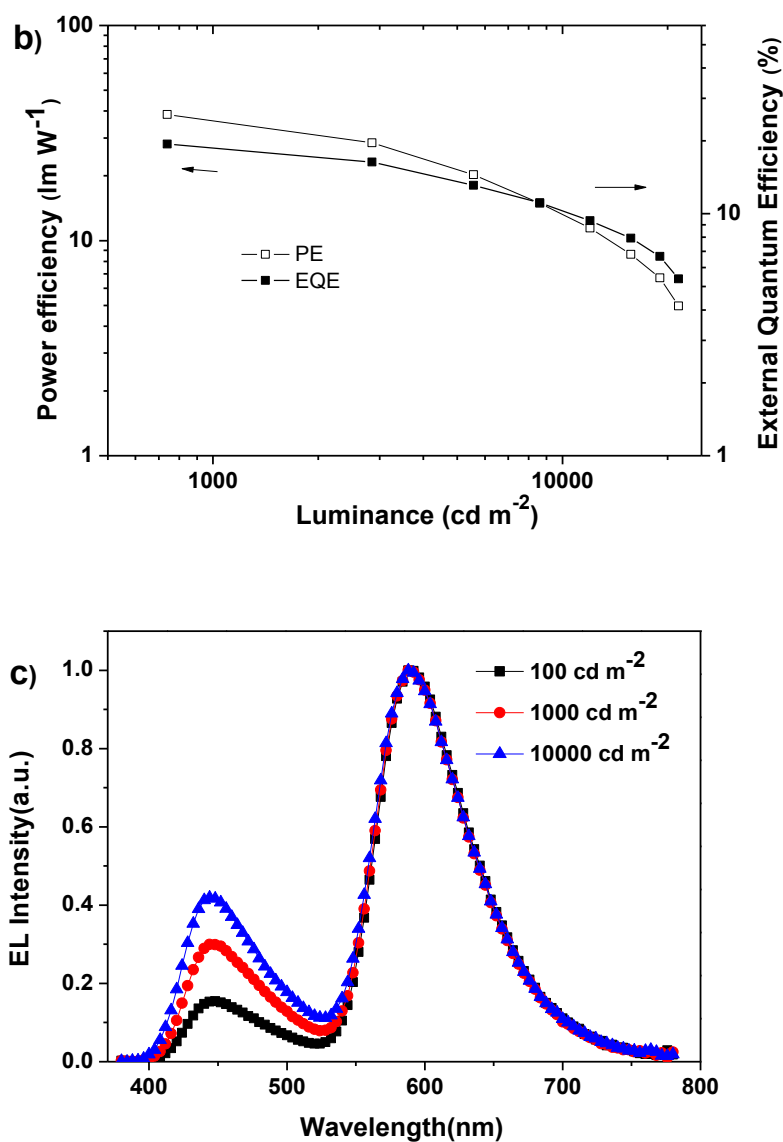
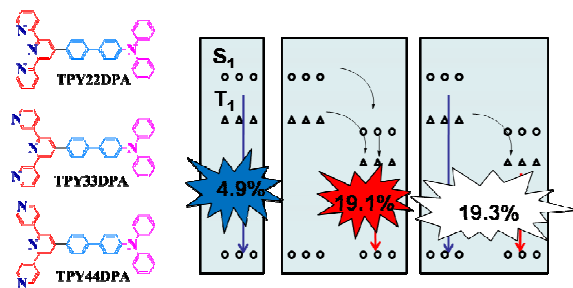


Figure 8. a) Current density-Luminance-Voltage characteristics of device W; b) PE-EQE-Luminance plots of device W; c) The EL spectra of device W.



A series of multifunctional fluorophores as highly efficient blue fluorescent emitters and red phosphorescent hosts.